Titre: Title:	Fate and inhibitory effect of silver nanoparticles in high rate moving bed biofilm reactors
Auteurs: Authors:	Sanaz Alizadeh, Subhasis Ghoshal et Yves Comeau
Date:	2019
Type:	Article de revue / Journal article
Référence: Citation:	Alizadeh, S., Ghoshal, S. & Comeau, Y. (2019). Fate and inhibitory effect of silver nanoparticles in high rate moving bed biofilm reactors. *Science of Total Environment*, *647*, p. 1199-1210. doi:10.1016/j.scitotenv.2018.08.073

The Science of the Total Environment, 647: 1199-1210.

doi : 10.1016/j.scitotenv.2018.08.073

Fate and inhibitory effect of silver nanoparticles in high rate moving bed biofilm reactors

Sanaz Alizadeh[1], Subhasis Ghoshal[2], Yves Comeau[1]

[1]Department of Civil, Geological and Mining Engineering, Polytechnique Montreal, 2500 Polytechnique road, Montreal (Quebec) Canada H3T 1J4

[2] Department of Civil Engineering and Applied Mechanics, McGill University, 817 Sherbrooke Street West, Montreal (Quebec) Canada H3A 0C3

ABSTRACT

Municipal water resource recovery facilities are the primary recipients of a significant fraction of discharged silver nanoparticle (AgNP)-containing wastes, yet the fate and potential risks of AgNPs in attached-growth biological wastewater treatment processes are poorly understood. The fate and inhibitory effects of polyvinylpyrrolidone (PVP)-coated AgNPs at environmentally-relevant nominal concentrations (10, 100, 600 μg/L) were investigated, for the first time, in high rate moving bed biofilm reactors (MBBRs) for soluble organic matter removal. The behavior and removal of continuously added AgNPs were characterized using single-particle inductively coupled plasma mass spectrometry (spICP-MS). While no inhibitory effect at average influent concentration of 10.8 μg/L Ag was observed, soluble COD removal efficiency was significantly decreased at 131 μg/L Ag in 18 days and 631 μg/L Ag in 5 days with suppressed biofilm viability. The inhibitory effect of AgNPs on treatment efficiency was highly correlated to the retained mass of total Ag in attached biofilm on the carriers. Biofilm demonstrated limited retention capacity for AgNPs over 18 days. Considerable mass of Ag (38% to 75%) was released via effluent, predominantly as NPs. We detected some chemically transformed and potentially less toxic forms of silver nanoparticles (Ag_2S, AgCl), over the exposure period. This study demonstrated the distinct interaction dynamics, bioavailability and inhibitory effects of AgNPs in a biofilm system. Release of bioavailable AgNPs via effluent and AgNP-rich biofilm, sloughing off the carriers, can affect the treatment chain efficiency of downstream processes. Thus, the inhibitory effects of AgNPs can be a concern even at concentrations as low as 100 to 600 μg/L Ag in biological attached growth wastewater treatments.

Keywords: Silver nanoparticles, moving bed biofilm reactor, toxicity, single particle ICP-MS, dissolution.

1. Introduction

Silver nanoparticles (AgNPs) are the most widely used metal nanoparticles in various commercial products, cosmetics, food processing and also as an alternative disinfectant and anti-biofouling agent in various products and in industrial pipelines (*e.g.,* in the food, fermentation and water treatment industries), due to their effective antimicrobial properties (Huang et al., 2016; Liu et al., 2014; Patlolla et al.; 2012, Mohanta et al., 2017). Materials flow analyses of released AgNPs from personal care products, various household and industrial products suggest that a significant fraction of discharged AgNP-containing wastes enter municipal water resource recovery facilities (WRRFs) with an estimated influent concentration of AgNPs around 1.5 μg/L (Gottschalk et al., 2009; Li et al., 2010). Thus, WRRFs play an important role in controlling the release of such engineered nanoparticles (ENPs) into the environment by their liquid or biosolids discharges.

The toxicity of AgNPs to bacteria is caused by cell membrane damage, inactivation of key enzymes and DNA, and oxidative stress via the generation of reactive oxygen species (Durán et al., 2016). Given the antimicrobial activity of AgNPs, their potential inhibitory effects on microbial communities involved in biological wastewater treatment processes and the implications for treatment efficiencies cannot be overlooked. The inhibitory effect of AgNPs (0.1 to 20 mg/L) was extensively studied in suspended-growth systems over various exposure scenarios (20 to 70 days) (Alito and Gunsch, 2014; Yang et al., 2014; Zhang et al., 2016c). Attached-growth biological processes (e.g. moving bed biofilm bioreactors), however, are rarely investigated for the environmental fate and inhibitory effects of AgNPs.

Biofilm is comprised of different phenotypes and genotypes which impart specific biological activities, metabolic pathways, and stress responses (Stewart and Franklin, 2008). The

47 extracellular polymeric substances (EPS), primary components of the biofilm, play a crucial role
48 in both AgNP-biofilm interactions, subsequent diffusion of NPs into the biofilm and their
49 toxicity (Fabrega et al., 2009; Peulen and Wilkinson, 2011). A few recent studies have reported
50 the high retention of AgNPs by biofilm, inhibition of biofilm formation, biofilm structural
51 alteration, inactivation of metabolic activity, and reduction of the biofilm volume (Fabrega et al.,
52 2009; Mallevre et al., 2016; Park et al., 2013). These studies used mono-species biofilms at
53 different maturity stages with exposure time between 24 h to 96 h over a range of AgNPs
54 concentrations (1 to 100 mg/L). These toxicity experiments were conducted in simplified
55 biological media, under conditions that are not representative of typical WRRF process
56 conditions.

57 Various studies, including those discussed above, have used biological or toxicological endpoints
58 to evaluate the inhibitory effect of AgNPs on process efficiency and on microbial communities
59 but did not evaluate changes in AgNP characteristics such as size and composition, or their
60 dissolution. High concentration of dissolved oxygen and relevant pH (7.7 to 7.8) in aerobic
61 biological wastewater treatment processes provide thermodynamically favorable conditions for
62 oxidation and dissolution of AgNPs, influencing their dynamics, especially at low NP
63 concentrations (Azodi et al., 2016; Merrifield et al., 2017). Neither total Ag nor Ag^+
64 concentrations are sufficient predictors of AgNPs inhibitory effects (Azimzada et al., 2017).
65 Therefore, quantification of Ag in its NP and dissolved forms, in the compartments of interest,
66 are necessary for the validation and comprehensive understanding of the fate of AgNPs and their
67 mechanisms of toxicity in such complex environmental conditions.

68 Studies of the fate of AgNPs at environmentally relevant concentrations in complex
69 environmental matrices are scarce, due to the challenges of analytical methods. Single-particle

inductively coupled plasma mass spectrometry (spICP-MS) is an emerging analytical technique that is able to simultaneously characterize metal NP size distributions, particle number concentrations and dissolved metal concentrations at low NPs concentrations in complex, organic matter-rich, environmental matrices (Azodi et al., 2016; Mitrano et al., 2012; Pace et al., 2012).

The specific objectives of this study were to (1) characterize the retention and distribution behavior of AgNPs in aerobic attached-growth biological wastewater treatment process and to (2) determine the inhibitory effect of AgNPs on the COD removal efficiency and biofilm viability of a continuous exposure at nominal influent concentrations of 10 to 600 µg/L AgNPs. A lab-scale high-rate moving bed biofilm reactor (MBBR), for organic matter removal, was used in this study and fed with a synthetic soluble influent. The impact of AgNPs on the performance of the MBBRs was characterized in terms of soluble COD (S_{COD}) removal efficiency, effluent quality and biofilm viability over a period of 18 days. The biofilm membrane integrity was evaluated using a fluorescent microscopy technique with two DNA-binding stains (SYTO-9 and propidium iodide). The nanoparticle mean diameters, AgNP and dissolved Ag mass concentrations were simultaneously quantified in influent, bioreactor and effluent samples using spICP-MS to assess aggregation state, dissolution and distribution between different reactor phases. The retention capacity of the attached biofilm for Ag was estimated based on the cumulative total Ag mass balance. To the best of our knowledge, this is the first study evaluating the fate and toxicity of PVP-AgNPs at environmentally-relevant concentrations in attached-growth MBBR systems.

2. Materials and Methods

2.1. Reactor configuration

Three 1 L lab-scale MBBR reactors, operated in parallel under identical conditions, were fed with synthetic soluble influent (Fig. 1). Synthetic wastewater was used throughout the experimental phase to ensure constant influent characteristics and well-controlled conditions to identify the inhibitory effects of the PVP-AgNPs. The concentrated solution (2.5 g S_{COD}/L) was based on a recipe adapted from OECD (1976) to obtain a typical C/N/P ratio of 100/12/2 for a medium to high strength domestic wastewater (Metcalf & Eddy-AECOM, 2014) (Table 1). Sodium acetate, soy protein and peptone were used to mimic the readily-degradable carbonaceous content of wastewater (Table 1). The synthetic influent provided C, N, P and minerals to favor biofilm growth. The concentrated feed was pumped and diluted with tap water before entering the reactors to obtain a COD concentration of 250 mg S_{COD}/L at organic loading rate of 11.2 g COD m^{-2} d^{-1} of active surface area (Table 1) to be representative of the soluble fraction (without TSS) of a medium strength wastewater (Metcalf & Eddy-AECOM, 2014). Tap water was used as dilution water to provide additional minerals (Mg, Ca, etc.). The characteristics of the synthetic influent, after dilution of the concentrated solution, are presented in Table 2.

The reactors operated at a hydraulic retention time (HRT) of 1 hour, pH of 7.4 ± 0.1, a dissolved oxygen concentration (DO) of 6.5 ± 0.9 mg/L and 60% volumetric fill ratio with AnoxKaldnes K5 carriers (Veolia Water Technologies Canada Inc.) with a specific active surface area of 800 m^2/m^3. The carriers were kept in suspension by aeration. The air was humidified to compensate for evaporation from the reactors. In the preliminary start-up phase, all reactors were inoculated with K3 carriers, collected from the full-scale MBBR at the Mascouche Terrebonne WRRF (Quebec, Canada) for a period of five days to favor biofilm growth and to ensure the development of a representative microbial community of a WRRF (Brosseau et al., 2016).

Subsequently, the K3 carriers were removed from the reactors. The temperature was controlled at 21 ± 0.2 °C in the double-jacketed MBBRs by a circulator (Programmable Circulator 9712, PolyScience, USA).

2.2 PVP-AgNPs exposure to MBBRs

AgNPs (nanoparticles of Ag(0)), capped with 40 kDa PVP polymer, were purchased from Nanocomposix (Econix silver) in aqueous suspension with a stock concentration of 5.35 mg/mL and nominal diameter of 50 nm. SpICP-MS (PerkinElmer NexION 300X) analyses provided a mean diameter of 52 ± 0.5 nm. According to the AgNP product description, the zeta potential and surface area of AgNPs were -55 mV (at pH 4.6) and 10.7 m^2/g, respectively. The spherical shape of AgNPs was observed by transmission electron microscopy (TEM). All three reactors reached quasi steady-state conditions after about 30 days as indicated by a stable S_{COD} removal efficiency. Afterwards, the reactors were monitored for 45 days as a control period. Influent AgNP suspensions were prepared by dilution of PVP-AgNPs stock suspension in Milli-Q water and sonicated for 10 min to ensure that the NPs were dispersed. The AgNP influent suspensions were pumped to each reactor from day 76 at a constant flow rate (1.65 ± 0.03 mL/min), resulting in an average influent total Ag concentration of 10.8 ± 0.3 µg/L Ag ($MBBR_1$), 131 ± 7 µg/L Ag ($MBBR_2$) and 631 ± 27 µg/L Ag ($MBBR_3$) after dilution. The influent nanoparticle suspensions were replenished regularly. Characterization of particle size and concentration of influent AgNPs suspensions indicated the stability of NP in influent stock over every 72 h period. The average characteristics of influent in each MBBR (Table S2) were used for mass balance analysis.

The AgNP exposure experiment lasted 18 days in the MBBRs, during which the effluent water quality, attached biofilm viability and Ag distribution were monitored. Chemical oxygen demand (COD), total suspended solids (TSS) and volatile suspended solids (VSS) were measured

139 according to Standard Methods (APHA et al., 2012). Glass microfiber 1.2 µm filters
140 (Whatman® 934-AH™, GE Healthcare Life Sciences, USA) and 0.45 µm cellulose membrane
141 filters (MF-Millipore™, EMD Millipore, USA) were used for suspended solids and soluble COD
142 analyses, respectively.

143 **2.3 Biofilm total biological viability**

144 The inhibitory effect of AgNPs on biofilm membrane integrity was evaluated using the
145 Live/Dead *Baclight* bacterial viability kit (Molecular Probes, Invitrogen, Kit L13152) and
146 confocal laser scanning microscopy (CLSM) using the modified protocol of Young et al. (2016).
147 Three K5 carriers were randomly chosen in each reactor before and after exposure to AgNPs.
148 The carriers were cut to expose the inner surfaces and were kept in 2 mL of bioreactor
149 suspension that also contained suspended biomass, and placed in the special container for CLSM
150 imaging. The biofilm and suspended-biomass containing samples were stained with two DNA-
151 binding stains (SYTO-9 and propidium iodide). A minimum of 5 randomly-chosen microscopic
152 fields were scanned for CLSM. All fluorescence images of biofilm were obtained using a LSM
153 510 META Axioplan 2 confocal laser scanning microscope with 40X objective (Carl Zeiss; Jena,
154 Germany), equipped with 488 nm argon laser and 543 and 633 nm helium–neon lasers (Blanc et
155 al., 2005).

156 **2.4 Silver analyses**

157 **2.4.1 Total metal analysis**

158 The influent, bioreactor and effluent were sampled on days 76, 78, 81, 84, 89 and 94. Bioreactor
159 and effluent samples contained suspended flocs (50 to 150 mg TSS/L) but no K5 carriers. All
160 samples were homogenized for 30 s with a vortex mixer prior to total Ag analysis. Samples were
161 digested, in duplicate, using 65% nitric acid (HNO_3) and 30% hydrogen peroxide (H_2O_2) (ratio

of 5:1) on a hot digestion block at 95 ºC for 30 minutes (Yuan et al., 2015). The total Ag concentration was determined using a PerkinElmer NexION 300x ICP-MS in standard mode. Calibration solutions were prepared fresh prior to each analysis from a dissolved Ag standard of 1000 mg/L in 4% HNO_3 (PlasmaCAL). Each sample was measured in triplicate. Quality control (QC) samples (0.1 µg Ag/L in 2% HNO_3) were analyzed after every 10 samples. Ag recovery in the QC samples was between 99% to 105%.

2.4.2 AgNP characterization

AgNP concentration and size as well as dissolved Ag were determined simultaneously in aqueous samples (Fig. 2) by spICP-MS and data analyses was performed by the Syngistix nano application module (version 1.1) as described by Azodi et al. (2016). The homogenized samples were allowed to settle for about 30 to 45 s and the aqueous supernatant was collected thereafter for analysis. A dwell time of 100 µs and sampling time of 100 to 150 s were used. Instrumental and data acquisition parameters of the analysis are indicated in SI (Table S3). The minimum detectable AgNP concentration in deionized water was 10 ng/L (14200 particle/mL) for 50 nm AgNPs (95% recovery) and detection limit of dissolved Ag was about 30 ng/L in single particle mode. The detection limit for AgNP size was ~10 nm in deionized water by spICP-MS as determined in our prior study (Azodi et al., 2016).

2.4.3 Cumulative Ag mass balance

Ag mass balance was performed based on the total Ag in the influent, bioreactor and effluent (Fig. 2). No direct measurements were done on solid fractions of samples. The amount of total Ag associated with biomass, including the flocs (Ag_{floc}) and attached biomass ($Ag_{carrier}$), were calculated using the measured fractions of Ag in influent (Ag_{inf}), bioreactor (Ag_{bio}) and effluent (Ag_{eff}) (Fig. 2). The concentration of Ag associated with suspended floc (Ag_{floc}), for both the

effluent and bioreactor, was calculated using the aqueous phase Ag (*i.e.* AgNPs + dissolved Ag) obtained from spICP-MS analysis of the supernatant of the samples after settling and Ag from the total metal analyses of the homogenized samples (Eq.1).

$$[Ag_{floc}]_{ti} = [Ag]_{ti} - ([AgNPs] + [\text{ dissolved Ag}])_{ti} \quad (1)$$

Where $[Ag]_{ti}$ represents $[Ag_{eff}]_{ti}$ for effluent and $[Ag_{susp}]_{ti}$ for the bioreactor. The mass of Ag in influent ($M_{Ag,inf}$), bioreactor ($M_{Ag,bio}$) and effluent ($M_{Ag,eff}$) of each MBBR, for each time interval (Δt) were calculated from Equations 2 to 5. The mass of Ag in bioreactor consisted of the mass of Ag in the suspended phase of the bioreactor ($M_{Ag,susp}$) and the retained mass of Ag by attached biofilm on the carrier ($M_{Ag,carrier}$). As shown in Fig. 2, the suspended phase of bioreactor included both concentrations of Ag in aqueous phase and suspended flocs (Ag_{floc}).

$$(M_{Ag,inf})_{ti} = (Q_{inf})_{ti} * [Ag_{inf}]_{ti} * (t_i - t_{i-1}) \quad (2)$$

$$(M_{Ag,eff})_{ti} = (Q_{eff})_{ti} * [Ag_{eff}]_{ti} * (t_i - t_{i-1}) \quad (3)$$

$$(M_{Ag,susp})_{ti} = V_{bio} * [Ag_{susp}]_{ti} \quad (4)$$

$$(M_{Ag,bio})_{ti} = (M_{Ag,inf})_{ti} - (M_{Ag,eff})_{ti} \quad (5)$$

Where Q_{inf} (L/day), Q_{eff} (L/day) and V_{bio} (L) are the flow rate of influent and effluent and volume of the bioreactor, respectively. In the final step, the retained mass of Ag by attached biofilm on the carrier ($M_{Ag,carrier}$) was estimated (Equation 6).

$$(M_{Ag,carrier})_{ti} = (M_{Ag,bio})_{ti} - (M_{Ag,susp})_{ti} \quad (6)$$

2.5 Statistical analysis

The statistical significance of differences between treatments ($p < 0.05$), before and after exposure to AgNPs, was evaluated using one-way repeated measures ANOVA in Statistica version 12 (StatSoft Inc., USA).

208 # 3. Results

209 ## 3.1 Effects of AgNPs on treatment efficiency

210 The S_{COD} removal efficiency was determined in three MBBRs, in response to the continuous
211 exposure to three nominal doses of 10, 100 and 600 µg/L AgNPs. Prior to exposure to AgNPs,
212 each MBBR was monitored for 30 days (day 45 to 75) under quasi steady state conditions as a
213 control period (Fig. 3). Effluent nitrate concentration remained around 0.4 mg N/L, showing no
214 significant nitrification occurring in the MBBRs as expected at such high rate conditions (results
215 not shown). Specific S_{COD} removal rate stabilized at 10.7 ± 0.2 g S_{COD} m^{-2} d^{-1}, 10.5 ± 0.3 g S_{COD}
216 m^{-2} d^{-1} and 9.9 ± 0.5 g S_{COD} m^{-2} d^{-1}, corresponding to a S_{COD} removal efficiency of $89\% \pm 0.5\%$,
217 $89\% \pm 0.3\%$ and $89\% \pm 1.4\%$ in $MBBR_1$, $MBBR_2$ and $MBBR_3$, respectively, over the control
218 period. After the start of AgNP addition, at average measured concentration of 10.8 ± 0.38 µg/L
219 Ag in its influent, $MBBR_1$ maintained an average S_{COD} removal efficiency of $89\% \pm 1.5\%$ over
220 the 18-day exposure period. Therefore, S_{COD} removal efficiency was not significantly affected
221 ($p > 0.05$) over an 18-day continuous exposure to influent concentration of 10.8 µg/L Ag in the
222 influent (Fig. $3A_1$).

223 At higher concentrations of AgNPs (100 and 600 µg/L), two phases were observed for MBBR
224 response to AgNP exposure. An unperturbed phase comprised the time interval after injection of
225 AgNPs, in which the biological activity of biofilm bacteria remained stable with no significant
226 impact of AgNPs. A second phase corresponded to the period during which the biomass was
227 significantly inhibited. Unperturbed phases of 96 h and 48 h were observed in $MBBR_2$ (131 ± 7
228 µg/L Ag) and $MBBR_3$ (631 ± 27 µg/L Ag), respectively. The second phase started thereafter
229 (Fig. $3A_2$-A_3) where the effluent S_{COD} gradually increased, decreasing the S_{COD} removal
230 efficiency significantly ($p < 0.05$) by about 22% over 12 days in $MBBR_2$ and 25% after 3 days in

231 $MBBR_3$ (Fig. 3B). Therefore, soluble COD removal efficiency was significantly decreased to
232 66% ± 0.7% in 18 days in $MBBR_2$ (131 ± 7 µg/L Ag) and to 64% ± 2.8% in 5 days in $MBBR_3$
233 (631 µg/L Ag). The significant increase of TSS concentration in effluent, in both systems
234 receiving 131 and 631 µg/L Ag (Fig. 3C) indicated significant detachment of biofilm which was
235 likely due to the antibacterial properties of AgNPs and/or dissolved Ag.

236 **3.2 Effect of AgNPs on biofilm total biological viability**

237 The potential bactericidal effect upon introduction of AgNPs in the MBBRs on biofilm bacteria
238 was characterized in terms of cell membrane integrity using CLSM. The CLSM images of
239 stained biofilm, exposed to different dosages of AgNPs, demonstrated the concentration-
240 dependent inactivation of biofilm total biological viability (Fig. 4). The extent of viability
241 inhibition was from no significant detectable membrane integrity damage at the lowest
242 concentration (10.8 µg/L Ag) (Fig. $4A_2$) to a noticeable increase in the number of dead cells in
243 the presence of 131 µg/L Ag and 631 µg/L Ag during the exposure period (Fig. $4B_2$-C_2).

244 **3.3 Fate and transport of AgNPs**

245 **3.3.1 Total silver**

246 Ag retention efficiency was determined using the total silver concentration in the influent and
247 effluent of MBBRs, and is shown in Fig. 5. With an average influent total Ag concentration
248 ($[Ag_{inf}]$) of 10.8 ± 0.3 µg/L, $MBBR_1$ retained about 21% of $[Ag_{inf}]$ on day 76 which increased
249 to 65% of $[Ag_{inf}]$ in bioreactor by day 81 (Fig. 5A). Afterwards, the Ag retention efficiency
250 stabilized at 52% ± 5% by day 94. $MBBR_2$, receiving Ag_{inf} concentration of 131 ± 7 µg/L,
251 demonstrated higher retention efficiency of Ag over the first 5 days (Fig. 5B). More than 30% of
252 $[Ag_{inf}]$ were retained in $MBBR_2$ on day 76, which reached up to 85% of $[Ag_{inf}]$ on day 81. The

retention efficiency subsequently decreased to 54% from day 81 to day 84, likely due to saturation of biofilm outer layers by AgNPs and/or biofilm sloughing off from the surface of the carriers. Thereafter $MBBR_2$ recovered its capacity to retain about 55% ± 9% of [Ag_{inf}] from day 84 to day 94. A higher concentration of AgNPs affected the biomass in $MBBR_3$ receiving Ag_{inf} concentration of 631 ± 27 µg/L, differently (Fig. 5C). The highest retention efficiency of 47% was attained after 1-hour exposure (one HRT) on day 76. Afterwards, the retention capacity of biofilms dramatically declined resulting in retention efficiency as low as 5% in 48 hours (day 78), but the system was able to recover its ability to retain AgNPs up to 35% by day 79 but fluctuated, changing to 20% over 24 hours by day 80.

The cumulative mass of total Ag, loading in the influent ($M_{Ag_{inf}}$), effluent ($M_{Ag_{eff}}$) and attached biofilm ($M_{Ag_{carrier}}$) are shown in Fig. 6A. Cumulative Ag mass balance was about 98% in all three reactors with negligible mass of Ag in the suspended phase of MBBRs. Attached biofilm retained 62% of $M_{Ag_{inf}}$ (0.79 mg) in $MBBR_1$ and 78% of $M_{Ag_{inf}}$ (12.14 mg) in $MBBR_2$ by day 81, which slightly decreased afterward. Retention of 54% of cumulative $M_{Ag_{inf}}$ (2.3 mg $Ag/m^2{}_{active\ surface}$) and 61% of cumulative $M_{Ag_{inf}}$(33 mg $Ag/m^2{}_{active\ surface}$) were observed by attached biofilm ($Ag_{carrier}$) in $MBBR_1$ and $MBBR_2$, respectively, by day 94. In $MBBR_3$, the mass balance suggests that more than 75% of cumulative $M_{Ag_{inf}}$ (43 mg) was released via the effluent over 5-day exposure indicating poor retention capacity of biofilm at higher AgNP concentrations (Fig. 6A).

3.3.2 AgNPs

Concentrations of AgNPs, and dissolved Ag were measured simultaneously in influent suspensions (Table S2) and the aqueous phase of samples collected from the MBBR bioreactors

(Fig. S1A-C) and the effluents (Fig. 5), using spICP-MS. For $MBBR_1$ (Fig. 5A, bar graphs), receiving an average influent concentration of 8.1 ± 2.3 µg/L AgNPs ($[AgNP_{inf}]$) and mean diameter of 48 ± 3 nm, its effluent contained 7.4 ± 0.2 µg/L and 3.3 ± 0.2 µg/L AgNPs on days 76 and 78, respectively (Fig. 5A). Over the first 48 hours of exposure, a larger cumulative fraction of $[Ag_{eff}]$ (78% to 87%) was detected in NP form in the aqueous phase of the effluent ($AgNP_{eff}$) with mean diameter in the range of 49 ± 0.4 to 52 ± 0.6 nm (Fig. S1D). Concentrations of $AgNP_{eff}$ were depleted afterwards. On day 81, $[AgNP_{eff}]$ (0.15 ± 0.01 µg/L), with mean diameter of 40 ± 0.5 nm, represented less than 4% of $[Ag_{eff}]$ indicating significant association of AgNPs to TSS_{eff}. Thereafter $[AgNP_{eff}]$ concentration increased and represented an average 61% of $[Ag_{eff}]$ (3.2 ± 0.7 µg/L AgNPs), with mean diameter from 35 ± 1 to 48 ± 0.2 nm, between day 89 and day 94.

For $MBBR_2$, receiving an average $AgNP_{inf}$ concentration of 75 ± 7 µg/L of a mean diameter of 47 ± 2 nm, a similar evolution in the distribution of AgNPs was observed in the effluent (Fig. 5B). A concentration of 83 ± 2 µg/L $AgNP_{eff}$ was measured after one-hour continuous exposure to AgNPs (one HRT), constituting 91% of detected $[Ag_{eff}]$ with mean diameter of 53 ± 0.1 nm (Fig. S1D). Following a decrease in $[Ag_{eff}]$, 19.5 ± 0.2 µg/L Ag_{eff} was released on day 81 where $[AgNP_{eff}]$ (9.4 ± 0.1 µg/L with mean diameter of 46 ± 0.1 nm) accounted for 48% of $[Ag_{eff}]$ and remaining 43% of $[Ag_{eff}]$ (8.6 µg/L) was associated with the effluent suspended solids, with a relatively small mass fraction accounted for by the dissolved concentration of Ag_{eff}. As the $[Ag_{eff}]$ increased thereafter, the major fraction of released silver was in the form of AgNPs (79% ± 2% of $[Ag_{eff}]$) with mean diameter of 47 ± 6 nm (Fig. S1D).

For $MBBR_3$ (Fig. 5C), receiving an average $AgNP_{inf}$ concentration of 442 ± 26 µg/L of mean diameter of 49 ± 1 nm, more than 85% of released $[Ag_{eff}]$ (289 ± 5 µg/L) was detected as $AgNP_{eff}$ over the first hour exposure. Along with the significant increase in $[Ag_{eff}]$ concentration by day 78 (48 h), likely due to significant increase of TSS_{eff}, $[AgNP_{eff}]$ (293 ± 8 µg/L) represented about 50% of the $[Ag_{eff}]$. No significant change was observed in mean diameter (Fig. S1D). For later sampling times, such as day 81, spICP-MS analysis was not feasible due interferences from the high concentration of suspended solids.

3.3.3. Dissolved Ag

Average dissolved Ag_{inf} concentrations of 2.5 ± 0.6 µg/L, 14.4 ± 6.0 µg/L and 39 ± 19 µg/L were measured in influent of $MBBR_1$, $MBBR_2$ and $MBBR_3$, respectively, indicating AgNP dissolution of 23%, 11% and 6% in influent NP stock solution (Table S2). SpICP-MS analyses showed variations in dissolved Ag concentrations over time in the effluent of both $MBBR_1$ and $MBBR_2$, whereas less than 7% of $[Ag_{eff}]$ were measured in dissolved form in $MBBR_3$ over the short exposure time (Fig. 5D). The maximum dissolved Ag concentration of 1.30 ± 0.04 µg/L (30% of $[Ag_{eff}]$) and 8.7 ± 1.0 µg/L (21% of $[Ag_{eff}]$) were measured in the effluent of $MBBR_1$ and $MBBR_2$, respectively, over the first 48 h (Fig. 5A, B, D). Afterwards, dissolved Ag concentration decreased and stabilized at about 20% of $[Ag_{eff}]$ in $MBBR_1$ and 10% of $[Ag_{eff}]$ in $MBBR_2$ by day 94 (Fig. 5D). Measured dissolved Ag in influent NP suspensions, entering reactors via separate constant flow, is likely in form of Ag^+ as AgNPs suspensions were prepared in pure water. However, the detected dissolved Ag in bioreactor and effluent samples are likely partially or completely complexed via interaction with suspended biomass.

4. Discussion

4.1 Inhibitory effect of AgNPs on S_{COD} removal efficiency and biofilm viability

The concentration-dependent inhibitory effect of AgNPs on S_{COD} removal efficiency was observed at nominal influent concentrations of 100 and 600 µg/L AgNPs in high rate MBBRs. These results are in contrast with recent studies. It is reported that the environmentally relevant concentration of 100 µg/L AgNPs had no adverse effects on carbon removal and bacterial activities of activated sludge over a 50-day exposure in a sequencing batch reactor process (Zhang et al., 2016c) and over a 65-day exposure in a membrane bioreactor (Zhang et al., 2014). These contrasting results could be due to differences between the process configurations, such as completely mixed versus batch system with different oxygen demand, sludge retention time, HRT, biomass characteristics and the size and coating of the AgNPs used under distinct experimental conditions. The process configuration governs biomass growth processes and determines the stability and transformation of AgNPs in the process and the bioavailability of Ag and their consequent impact on the wastewater microbial communities (Zhang et al., 2016a).

Attached growth processes such as in an MBBR, provide higher biomass concentrations (with larger specific surface area) in smaller reactor volumes as compared to suspended growth process such as activated sludge (Barwal and Chaudhary 2014). Therefore, higher biomass surface area/volume ratio in MBBR enhances the deposition rate and the mass transport of AgNPs to attached biomass, leading to enhanced Ag retention per unit weight of biomass in the reactor, compared to activate sludge systems. This results in relatively high toxicity even at lower influent concentrations. Our mass balance analysis indicated the accumulation of 3.2 mg Ag/$gVSS_{biofilm}$ in 5 days in $MBBR_3$ (631 µg/L Ag influent) and 4.9 mg Ag/$gVVS_{biofilm}$ in $MBBR_2$ (131µg/L Ag influent) over 18 days. In contrast, Zhang et al. (2016c) reported the

accumulated concentration of 0.47 mg Ag/gVSS in activated sludge, collected from a sequencing batch reactor (100 μg/L AgNPs influent) over 50 days. The significant accumulation and associated mass transport of Ag through the protective biofilm EPS into deeper layers of biofilm can result in toxicity to the biofilm biomass. The AgNPs transported into the biofilm can undergo dissolution delivering toxic Ag^{+} directly to adherent cells. The inhibitory effect of AgNPs at doses of both 131μg/L and 631μg/L Ag was correlated also to the loss of active biofilm via detachment due to metabolic stress and the accumulation of AgNPs over time within the biofilm.

The observed variation in inhibition effects of AgNPs at similar nominal influent AgNP concentrations can also be correlated to the differences in specific exposure conditions of activated sludge systems reported elsewhere (Zhang et al., 2014; Zhang et al., 2016c). In these studies AgNPs suspensions were injected into the anoxic chamber with the mixed liquor recirculation between the aerobic chamber and the anoxic chamber. This resulted in AgNPs first being exposed to a 2 h anoxic stage where there would have been considerable loading of organic matter on the AgNP surface which would have made AgNP susceptible to changes in aggregation state, oxidation state, precipitation of secondary phases and sorption of (in)organic species before reaching the aerobic zone. Wastewater ligands and ions (e.g., HS^{-}, Cl^{-}, SO_4^{2-}, HPO_4^{2-}) would react with injected AgNPs and dissolved Ag and form the silver complexes/precipitates**,** leading to reduced bioavailability (Behra et al., 2013). Simultaneously, AgNPs in the activated sludge could be transformed into Ag–sulfhydryl complexes and Ag_2S during the short anoxic phase, and therefore, reduce their toxicity (Doolette et al., 2013; Yuan et al., 2015). The lack of dissolved oxygen, and the abundance of organic matter bound to the AgNPs in the anoxic state would also decrease the subsequent dissolution of Ag in both the anoxic and aerobic zone. In our study the AgNPs stock suspensions were pumped directly to

each reactor (aerobic zone), enabling dissolution at all times, and thus distinct inhibitory level would be expected. Furthermore, Barker et al. (2018) suggested that the expected toxicity of AgNPs should not be based solely on the AgNP concentration in the wastewater influent or even the total mass load but rather on a more complex combination of factors including the influent AgNP concentration, total mass loading and the exposure time.

The inhibitory effect of AgNPs on treatment efficiency was highly correlated ($0.89 < R^2 < 0.98$) to the retained mass of Ag in the carriers ($Ag_{carrier}$) (Fig. 6B). The bioavailability and toxicity of retained AgNPs in the porous structure of biofilm are highly dependent upon their diffusivity in biofilm-laden systems and their interactions with the surface of bacteria (Peulen and Wilkinson, 2011). The lack of significant adverse effects on treatment efficiency of $MBBR_1$ at low concentrations of AgNPs, is likely due to the lower than threshold concentration for toxicity of AgNPs and Ag^+, or due to the complexation of Ag^+ to biological macromolecules and the sorption of those macromolecules to AgNPs in the biofilm EPS, reducing the diffusive flux of AgNPs and Ag^+ within the biofilm layers and reduce their toxicity (Kroll et al., 2014). Hindered nanoparticle diffusion in biofilms was demonstrated by Peulen and Wilkinson (2011). The interaction between EPS molecules and AgNPs results in the formation of stable complexes on the surface of AgNPs (*e.g.* corona effect) which could reduce the bioavailability and toxicity of AgNPs (Wirth et al., 2012). As in the case of $MBBR_2$ and $MBBR_3$, exposure to higher concentrations of AgNPs can lead to significant accumulation and mass transfer of AgNPs into deeper layers of biofilm.

Significant increase of TSS concentration in effluent of $MBBR_2$ and $MBBR_3$, due to the detachment of biofilm from the carriers, was highly correlated ($0.92 < R^2 < 0.99$) to the retained mass of Ag in the carriers ($Ag_{carrier}$) (Fig. 6C). The thinning effect of AgNPs on the biofilm (i.e.,

detachment and release of outer layers was reported at AgNPs concentrations higher than 200 μg/L (Fabrega et al., 2009), but was achieved at 131 μg/L Ag in this study. The interaction of AgNPs with an EPS matrix can potentially interfere with the cell to cell adhesion to the surface due to its cell wall destabilizing properties as an antimicrobial agent (Goswami et al., 2015). Grün et al. (2016) suggested that the complexation of Ag^+ and binding to AgNP surfaces by carboxyl, hydroxyl and amine macromolecules in EPS can impair interactions which mediate adhesion of the biofilm to surfaces, leading to diminished cohesive forces within the biofilm matrix. Thus, the biofilm detachment not only can inversely affect the treatment efficiency but also it can increase the risk of environmental exposure of AgNPs via the release of retained nanoparticles by detached biomass in the treated effluent.

Membrane integrity of the intact cells defines their potential metabolic activity whereas the cells with damaged membranes can be classified as permeabilized/dead cells (Foladori et al., 2010). The concentration-dependent alteration of membrane permeability and inactivation of attached biofilm were observed in MBBRs. Both AgNPs and the bioavailable dissolved Ag, released from the oxidative dissolution of AgNPs, and could have damaged the membrane integrity of attached biofilm at influent concentrations of 131 and 631 μg/L Ag which was consistent with S_{COD} removal efficiency loss in corresponding reactors. AgNPs up to 80 nm have demonstrated the ability to penetrate the outer membrane of bacteria (Morones et al., 2005). The large surface/volume ratio and special binding sites of AgNPs enhance the particle/cell surface contacts (Auffan et al., 2009). Upon attachement of AgNPs on to cell membrane, (a) released Ag^+ from oxidative disslution, can interact with thiol-containing proteins in the cell wall and destabilize the outer membrane of cells by an accumulation of immature membrane precursor proteins (Mirzajani et al., 2011) and (b) AgNP-induced oxidative stress can damage the cell

membrane by the generation of reactive oxygen species (ROS), leading to cell membrane integrity disruption and decomposition (Durán et al., 2016).

Contradictory results have been reported recently regarding the AgNP-induced membrane integrity damage and inhibition of viable biofilm. The inhibitory effect of AgNPs, with mean particle size of 50 nm, is reported at concentration as low as 5 µg/L towards *P. aeruginosa* biofilms over 24 h exposure (Kalishwaralal et al., 2010) whereas a number of studies reported considerably higher concentrations for inhibition or deactivation of biofilms. Fabrega et al. (2009) reported no significant effect of AgNPs (mean diameter of 65 nm) on *P. aeruginosa* biofilm viability at concentrations between 20 to 2000 µg/L of AgNPs over 24 h exposure time. Similarly, Sheng and Liu (2011) suggested the high tolerance of attached biofilms in wastewater over 24 h exposure to 200 mg/L AgNPs. This observed difference is likely due to disparity between the biological and structural properties of biofilm and the nature of the AgNPs used under distinct experimental conditions, particularly the exposure time. The physicochemical characteristics of NPs (size and coating) and the nature and age of the biofilm highly influence their diffusion coefficient. Peulen and Wilkinson (2011) suggested that as the density of biofilm increases with age, the pore size distribution shifts to smaller pore sizes altering deposition and bioavailability of AgNPs in denser, more developed biofilm.

4.2 Behavior of PVP-AgNPs in biofilm-laden media

The bioavailability of AgNPs is highly dependent on their chemical speciation, size-dependent diffusive fluxes and their particle coatings (Azimzada et al., 2017; Azodi et al., 2016). No evidence of aggregation was observed in the effluent of the three reactors, with no significant change in particle size (Fig. S1D). Mitzel and Tufenkji (2014) also reported a high stability of PVP-AgNPs in suspension and little change in their size or electrophoretic mobility with changing ionic

433 strength. The steric stabilization of AgNPs by PVP polymers typically prevents the particle
434 aggregation over a range of pH values and ionic strength (Song et al., 2011).

435 Despite the initial high retention capacity of biofilm for AgNPs, $MBBR_1$, $MBBR_2$ and $MBBR_3$
436 released 38%, 46% and 75% of the cumulative mass of Ag via their effluent over long-term
437 exposure scenarios (at effluent concentration of 0.05 to 0.5 mg/L, Fig. 5). The cumulative mass
438 released from the reactors was calculated from the measured effluent concentrations and the flow
439 rates. Approximately 55% to 79% of concentration of released total silver in the effluent of the
440 reactors ($[Ag_{eff}]$) was in the form of NPs and about 7% to 31% of $[Ag_{eff}]$ (1.14 to 24.5 µg/L) as
441 dissolved Ag. Herrling et al. (2016) also reported high retention capacity of heterotrophic biofilms
442 only at short exposure times (up to 3 h) over 27-day exposure in MBBR before release of silica-
443 coated iron oxide nanoparticles by the detachment of loaded biofilms. It is likely that association
444 with biomass is the main retention pathway of AgNPs in reactors receiving lower concentrations
445 of AgNPs (10 to 100 µg/L AgNPs). At higher concentrations (600 µg/L AgNPs), however, other
446 mechanisms affect the attachment efficiency of AgNPs to the biofilm surface (Mitzel and
447 Tufenkji, 2014). The initial high retention of PVP-AgNPs by the attached biofilm (Fig. 5)
448 suggests a high affinity of PVP-AgNPs for uncoated surfaces of biofilm via hydrophobic
449 interactions between hydrophobic PVP coatings of AgNPs and heterogeneously amphiphilic
450 surface of biofilm (Song et al., 2011). In longer-term exposure scenarios, however, as the
451 concentration increases in the bioreactor, the saturation of biofilm outer layers by local
452 accumulation of the nanoparticles and biofilm sloughing off from the surface of the carriers can
453 reduce the retention capacity of biofilm.

454 The inhibitory effect of AgNPs is ascribed to both nanoparticle and dissolved ions released from
455 AgNPs; however which fraction dominates toxicity appears inconclusive (Beer et al., 2012;

456 Navarro et al., 2008; Kawata et al., 2009). Most previous studies, reporting the Ag^+-mediated
457 toxicity of AgNPs, used silver nitrate ($AgNO_3$) as a source of bioavailable free Ag^+ ions at
458 concentration of 0.05 to10 mg/L in simple growth media (Beer et al., 2012; Choi et al., 2017). In
459 our study, the inhibitory effect of AgNPs was observed in $MBBR_2$ (131 µg/L Ag) and $MBBR_3$
460 (630 µg/L Ag) with an average influent dissolved Ag concentrations of 14.4 ± 6.0 µg/L
461 (11% [Ag_{inf}]) and 39 ± 19 µg/L (6% [Ag_{inf}]) respectively which were lower than the reported
462 inhibitory dissolved Ag concentrations (Beer et al., 2012; Choi et al., 2017). The detected
463 dissolved Ag in bioreactors, $MBBR_2$ (5 to 11 µg/L) and $MBBR_3$ (24 to 56 µg/L) (Fig. S1) were
464 likely partially or completely complexed via interaction with suspend biomass. Although
465 significant accumulation and mass transfer of AgNPs into deeper layers of biofilm would deliver
466 toxic Ag^+ directly to adherent cells via the (interfacial) dissolution of the surface-bound NPs in
467 biofilm matrix. Therefore, the measured dissolved Ag content in each reactor could not be fully
468 be attributed to the observed toxicity, and the presence of AgNP accounts for some part of the
469 toxicity of AgNPs, and is consistent with previously reported studies (Navarro et al., 2008;
470 Kawata et al., 2009). Apart from extracellular dissolution in media, diffused AgNPs in biofilm
471 EPS can partly follow a "Trojan-horse" type of mechanism (Hsiao et al., 2015). Cell surface-
472 associated AgNPs serve as carriers that penetrate cell membranes and dissolve to release a large
473 amount of bioavailable Ag^+ intracellularly, able to interact with cell molecules and damage cell
474 functions (Park et al., 2010; You et al., 2018); however the current knowledge on the mechanism
475 by which AgNPs interact with the cytosol environment and the dissolution properties of
476 intracellular AgNPs remains limited (You et al., 2018).

477 Our results suggest a concentration-dependent dissolution regime where the higher dissolution,
478 in terms of the fraction of Ag dissolved relative to total Ag added, is higher at lower

concentration of AgNPs (10 and 100 μg/L) in the effluent of reactors which is consistent with previous studies (Azodi et al., 2016; Hadioui et al., 2013; Zhang et al., 2016b). The lower percentage of dissolved Ag at higher influent concentration is likely due to high proton depletion (Liu and Hurt, 2010). The observed dissolution pattern in MBBR effluent (Fig. 5D) was consistent with the proposed two-phase dissolution kinetics, including a short, initial phase with a high release rate, and a longer, second phase with more gradual release (Mitrano et al., 2014). The dissolution behavior of AgNPs depends on the chemistry of the aqueous medium (*e.g.,* ionic strength, pH), the characteristics of NPs (e.g., size, particle concentration) as well as the nature of the surface capping agents (Azodi et al., 2016). PVP-coated AgNPs comprise an inner hard sphere of AgNPs covered with a relatively thick coating of high molecular weight PVP polymer which is uncharged with an amide group that also favors dissolution (Song et al., 2011). Azodi et al. (2016) attributed the decrease in dissolved Ag concentrations in the wastewater effluent samples to the reformation of the secondary NPs from dissolved Ag. We detected changes in chemistry of the particles (Ag_2S, AgCl) in the effluent of all MBBRs using TEM-EDS analysis (Fig. S2).

Sulfidation of AgNPs, may lead to the formation of partly sulfidated (Ag(0)/Ag_2S) or fully sulfidated (Ag_2S) particles, with the latter being formed at high sulfide concentrations existing in anaerobic environments. For partially sulfidated AgNPs, dissolution of Ag(0) with release of Ag^+ can occur (Zhang et al., 2018). In our reactors, the influent sulfate (SO_4^{2-}, 16.3 μM, in concentrated feed), as the only source of sulfur, needs to be reduced to bisulfide (HS^-) by sulfate-reducing bacteria as an essential step for the sulfidation of AgNP. Only anoxic/anaerobic zones, within the lower layers of biofilm, could favor the growth of sulfate-reducing bacteria (Auvinen et al., 2017). Due to high concentration of dissolved oxygen (6.5 mg O_2/L) and lack of enough

electron donors (low concentration of organic compounds), an incomplete sulfate reduction is expected. Therefore, considering the low ratio of S/Ag (0.037 to 0.25, based on 10% influent sulfate reduction) in our reactors, and the presence of dissolved Ag at concentrations ranging from 1.14 to 56 µg/L (bioreactor) it may be concluded that although sulfidation of AgNPs occurred, it did not cause Ag to be unavailable to bacteria and did not prevent toxicity.

The sulfidation of AgNPs, even in the presence of strong capping agents such as PVP, is proposed as the final thermodynamic fate of AgNPs, which can minimize the concentration of dissolved Ag (Levard et al., 2011; Liu and Hurt, 2010). The non-uniform sulfidation of AgNP surface, however, may still contribute to NP dissolution (Kent et al., 2014). In parallel, the influent chloride (12.5 mM in concentrated feed, Table 1) can act as a sink for Ag^+ ions released from oxidative dissolution of PVP-AgNPs by forming insoluble AgCl(s) species at low Cl^- concentrations and soluble chloro-silver complexes (i.e., $AgCl_2^-$, $AgCl_3^{2-}$, $AgCl_4^{3-}$) at high Cl^- concentrations (Azodi et al., 2016; Zhang et al., 2018) leading to a high Ag^+ gradient between the surface of AgNPs and a bulk solution that further favor the dissolution of AgNPs. It should be noted that AgNP bioavailability in biological matrices can be highly influenced by the complexation/competition with components in the wastewater effluent. The release of AgNP-rich biofilm, sloughed of the carrier surface can adversely affect the efficiency of downstream treatment chains such as nitrifying MBBRs. Thus, the potential impact of AgNPs in the receiving environment would still be a concern even at proposed environmental concentrations.

The risks associated with exposure to AgNPs during wastewater treatment, can be attenuated by possible changes in their aggregation state, surface composition, their reactivity. Coagulation-flocculation process and chemical precipitation for treatment of the AgNP-containing stream can likely increase their hetero-aggregation, leading to lower Ag bioavailability prior the biological

525 treatment in WRRFs. Folens et al. (2017) reported the high efficiency of an poly aluminum
526 chloride coagulant in combination with a pH-correction and an anionic polyelectrolyte as
527 flocculant as an effective combination for Ag removal in wastewater matrix. Downstream of
528 biological process, incorporation of reactive media such as slag filters (Claveau-Mallet et al.,
529 2013) can potentially reduce the Ag via complexation/precipitation reactions with the widely
530 present inorganic and organic substances. There is a need to evaluate the efficacy of such
531 approaches and to understand how NPs behave under such conditions.

532 **Conclusion**

533 This study was focused on assessing the sensitivity of attached-growth biological wastewater
534 treatment processes at environmental relevant concentrations of AgNPs. This is the first study
535 that investigated the fate and inhibitory effect of PVP-AgNPs in high rate carbon removal
536 MBBRs, at nominal concentrations of 10 to 600 µg/L AgNPs. Although previous studies
537 suggested no lethal impact of certain nanoparticles (e.g. CeO_2, TiO_2, CuO and AgNPs) on
538 biofilm system, our results indicated the adverse effect of PVP-AgNPs on structural and
539 functional response of the biofilm in MBRR which was dependent on the exposure time and
540 influent Ag concentration. Suppressed soluble COD removal efficiency and biofilm membrane
541 integrity damage in reactors could affect the stability of such high-rate treatments. The observed
542 significant biofilm detachment from the surface of the carriers could affect the sludge retention
543 time of the reactors and the biomass specialization. The quantitative characterization of
544 nanoparticles in MBBRs, using spICP-MS, and Ag mass balance indicated the limited retention
545 capacity of aerobic heterotrophic biofilm for AgNPs over long term exposure. Our findings
546 imply lower efficiency of MBBRs to retain AgNPs compared to the commonly used activated
547 sludge systems. The release of AgNP-rich biofilm, sloughed off the carriers, could affect the

548 treatment chain efficiency of a downstream nitrifying MBBR or the effluent receiving stream.
549 Our results stress the need for strategies to control the release of such NPs from biofilm systems.
550 This study contributes to a better understanding of the fate and behavior of AgNPs in biological
551 wastewater processes, providing key information that can be used to predict the environmental
552 risks of ENPs (transport, persistence and toxicity) in aquatic ecosystems.

553 **Acknowledgements**

554 The authors thank the Natural Sciences and Engineering Research Council of Canada (Grant no.
555 STPGP 430659–12), Environment and Climate Change Canada, PerkinElmer Health Sciences
556 Canada, the Fonds de Recherche du Québec Nature et Technologies (FRQNT), the Canadian
557 Water Network (CWN), SNC Lavalin Environnment, the City of Calgary and the City of Saint-
558 Hyacinthe for their financial support. The authors thank Jean-Philippe Massé, Le Centre de
559 Caractérisation Microscopique des Matériaux of Polytechnique Montreal for TEM/EDS analysis,
560 Nicolas Tran-Khanh of Polytechnique Montreal for CLSM analyses, the Terrebonne/Mascouche
561 WRRF for assistance with wastewater sampling and Dr. Flavio Piccapietra of McGill for
562 assistance with spICP-MS analyses and data interpretation.

563 **References**

564 1. Alito, C.L., Gunsch, C.K., 2014. Assessing the effects of silver nanoparticles on biological
565 nutrient removal in bench-scale activated sludge sequencing batch reactors. *Environ. Sci.*
566 *Technol.* 48 (2), 970-9766.
567 2. APHA; AWWA; WEF, 2012. *Standard Methods for the Examination of Water and*
568 *Wastewater*, 22nd ed. American Public Health Association, American Water Works
569 Association & Water Environment Federation, Washington, D.C.
570 3. Auffan, M., Rose, J., Wiesner, M.R., Bottero, J.-Y., 2009. Chemical stability of metallic
571 nanoparticles: a parameter controlling their potential cellular toxicity in vitro. *Environ.*
572 *Pollut.* 157 (4), 1127-1133.
573 4. Auvinen, H., Kaegi, R., Rousseau, D. P., Du Laing, G., 2017. Fate of silver nanoparticles in
574 constructed wetlands—a microcosm Study. *Water, Air, & Soil Pollut.* 228 (3), 97.

5. Azimzada, A., Tufenkji, N., Wilkinson, K.J., 2017. Transformations of silver nanoparticles in wastewater effluents: links to Ag bioavailability. *Environ. Sci.: Nano* 4 (6), 1339-1349.
6. Azodi, M., Sultan, Y., Ghoshal, S., 2016. Dissolution behavior of silver nanoparticles and formation of secondary silver nanoparticles in municipal wastewater by single-particle ICP-MS. *Environ. Sci. Technol.* 50, 13318-13327.
7. Barker, L., Giska, J., Radniecki, T. and Semprini, L., 2018. Effects of short-and long-term exposure of silver nanoparticles and silver ions to *Nitrosomonas europaea* biofilms and planktonic cells. *Chemosphere* 206, 606-614.
8. Barwal, A. &Chaudhary, R., 2014. To study the performance of biocarriers in moving bed biofilm reactor (MBBR) technology and kinetics of biofilm for retrofitting the existing aerobic treatment systems: a review. *Rev. Environ. Sci. Bio.* 13(3), 285-299.
9. Beer, C., Foldbjerg, R., Hayashi, Y., Sutherland, D. S., Autrup, H., 2012. Toxicity of silver nanoparticles—nanoparticle or silver ion? *Toxicology letters 208 (3), 286-292.*
10. Behra, R., Sigg, L., Clift, M.J., Herzog, F., Minghetti, M., Johnston, B., Petri-Fink, A., Rothen-Rutishauser, B., 2013. Bioavailability of silver nanoparticles and ions: from a chemical and biochemical perspective. *J. Roy. Soc. Interface* 10(87), 20130396.
11. Blanc, A., Tran-Khanh, N., Filion, D., Buschmann, M. D., 2005. Optimal processing method to obtain four-color confocal fluorescent images of the cytoskeleton and nucleus in three-dimensional chondrocyte cultures. *J. Histochem. Cytochem.* 53 (9), 1171-1175.
12. Brosseau, C., Émile, B., Labelle, M.-A., Laflamme, É., Dold, P. L., Comeau, Y., 2016. Compact secondary treatment train combining a lab-scale moving bed biofilm reactor and enhanced flotation processes. *Water Res.* 106, 571-582.
13. Choi, Y., Kim, H.-A., Kim, K.-W. &Lee, B.-T., 2018. Comparative toxicity of silver nanoparticles and silver ions to *Escherichia coli*. *J. Environ. Sci.* 66, 50-60.
14. Claveau-Mallet, D., Wallace, S. and Comeau, Y. (2013) Removal of phosphorus, fluoride and metals from a gypsum mining leachate using steel slag filters. *Water Res.* 47(4), 1512-1520.
15. Doolette, C.L., McLaughlin, M.J., Kirby, J.K., Batstone, D.J., Harris, H.H., Ge, H., Cornelis, G.,2013. Transformation of PVP-coated silver nanoparticles in a simulated wastewater treatment process and the effect on microbial communities. *Chem. Cent. J.* 7(1), 46.
16. Durán, N., Durán, M., de Jesus, M. B., Seabra, A. B., Fávaro, W. J., Nakazato, G., 2016. Silver nanoparticles: a new view on mechanistic aspects on antimicrobial activity. *Nanomedicine: Nanotechnol., Biol. Medicine* 12 (3), 789-799
17. Fabrega, J., Renshaw, J.C., Lead, J.R., 2009. Interactions of silver nanoparticles with *Pseudomonas putida* biofilms. *Environ. Sci. Technol.* 43 (23), 9004-9009.
18. Foladori, P., Tamburini, S., Bruni, L., 2010. Bacteria permeabilisation and disruption caused by sludge reduction technologies evaluated by flow cytometry. *Water Res.* 44 (17), 4888-4899.
19. Folens, K., Huysman, S., Van Hulle, S., Du Laing, G., 2017. Chemical and economic optimization of the coagulation-flocculation process for silver removal and recovery from industrial wastewater. *Sep. Purif. Technol.* 179, 145-151.

20. Goswami, S., Sahareen, T., Singh, M., Kumar, S., 2015. Role of biogenic silver nanoparticles in disruption of cell–cell adhesion in *Staphylococcus aureus* and *Escherichia coli* biofilm. *J. Ind. Eng. Chem.* 26, 73-80.
21. Gottschalk, F., Sonderer, T., Scholz, R.W., Nowack, B., 2009. Modeled environmental concentrations of engineered nanomaterials (TiO_2, ZnO, Ag, CNT, fullerenes) for different regions. *Environ. Sci. Technol.* 43 (24), 9216-9222
22. Grün, A.Y., Meier, J., Metreveli, G., Schaumann, G.E., Manz, W., 2016. Sublethal concentrations of silver nanoparticles affect the mechanical stability of biofilms. *Environ. Sci. Pollut. Res. Int.* 23 (23), 24277-24288.
23. Hadioui, M., Leclerc, S., Wilkinson, K. J., 2013. Multimethod quantification of Ag^+ release from nanosilver. *Talanta* 105, 15-19.
24. Herrling, M.P., Lackner, S., Tatti, O., Guthausen, G., Delay, M., Franzreb, M., Horn, H., 2016. Short and long term biosorption of silica-coated iron oxide nanoparticles in heterotrophic biofilms. *Sci.Total Environ.* 544,722-729.
25. Hsiao, I.-L., Hsieh, Y.-K., Wang, C.-F., Chen, I.-C., Huang, Y.-J., 2015. Trojan-horse mechanism in the cellular uptake of silver nanoparticles verified by direct intra-and extracellular silver speciation analysis. *Environ. Sci. Technol.* 49(6), 3813-3821.
26. Huang, L., Zhao, S., Wang, Z., Wu, J., Wang, J., Wang, S., 2016. In situ immobilization of silver nanoparticles for improving permeability, antifouling and anti-bacterial properties of ultrafiltration membrane. *J. Membrane Sci.* 499, 269-281
27. Kalishwaralal, K., BarathManiKanth, S., Pandian, S.R.K., Deepak, V., Gurunathan, S., 2010. Silver nanoparticles impede the biofilm formation by *Pseudomonas aeruginosa* and *Staphylococcus epidermidis*. *Colloids and Surfaces B: Biointerfaces* 79 (2), 340-344
28. Kawata, K., Osawa, M., Okabe, S., 2009. In vitro toxicity of silver nanoparticles at noncytotoxic doses to HepG2 human hepatoma cells. *Environ. Sci. Technol. 43* (15), 6046-6051.
29. Kent, R.D., Oser, J.G., Vikesland, P.J., 2014. Controlled evaluation of silver nanoparticle sulfidation in a full-scale wastewater treatment plant. *Environ. Sci. Technol.* 48 (15), 8564-8572.
30. Kroll, A., Behra, R., Kaegi, R., Sigg, L., 2014. Extracellular polymeric substances (EPS) of freshwater biofilms stabilize and modify CeO_2 and Ag nanoparticles. *PLoS One* 9 (10), e110709.
31. Levard, C., Reinsch, B.C., Michel, F.M., Oumahi, C., Lowry, G.V., Brown Jr, G.E., 2011.Sulfidation processes of PVP-coated silver nanoparticles in aqueous solution: impact on dissolution rate. *Environ. Sci. Technol.* 45 (12), 5260-5266.
32. Li, W.-R., Xie, X.-B., Shi, Q.-S., Zeng, H.-Y., You-Sheng, O.-Y., Chen, Y.-B., 2010. Antibacterial activity and mechanism of silver nanoparticles on *Escherichia coli*. *Appl. Microbiol. Biotechnol.* 85 (4), 1115-1122.
33. Lin, H., Ye, C., Lv, L., Zheng, C. R., Zhang, S., Zheng, L., Zhao, Y., Yu, X., 2014. Characterization of extracellular polymeric substances in the biofilms of typical bacteria by the sulfur K-edge XANES spectroscopy. *J. Environ. Sci.* 26 (8), 1763-1768.

34. Liu, J., Hurt, R.H., 2010. Ion release kinetics and particle persistence in aqueous nano-silver colloids. *Environ. Sci. Technol. 44* (6), 2169-2175.
35. Liu, J., Pennell, K.G., Hurt, R.H., 2011. Kinetics and mechanisms of nanosilver oxysulfidation. *Environ. Sci. Technol.* 45 (17), 7345-7353.
36. Liu, X., Tang, B., Gu, Q., Yu, X., 2014. Elimination of the formation of biofilm in industrial pipes using enzyme cleaning technique. MethodsX 1, 130-136.
37. Mallevre, F., Fernandes, T.F., Aspray, T.J., 2016. *Pseudomonas putida* biofilm dynamics following a single pulse of silver nanoparticles. *Chemosphere* 153, 356-364.
38. Merrifield, R.C., Stephan, C., Lead, J., 2017. Determining the concentration dependent transformations of Ag nanoparticles in complex media: using SP-ICP-MS and Au@ Ag core–shell nanoparticles as tracers. *Environ. Sci. Technol.* 51, (6), 3206-3213.
39. Metcalf & Eddy-AECOM, 2014. *Wastewater Engineering: Treatment and Resource Recovery*. 5th ed., McGraw-Hill, New York.
40. Mirzajani, F., Ghassempour, A., Aliahmadi, A., Esmaeili, M.A., 2011. Antibacterial effect of silver nanoparticles on *Staphylococcus aureus*. *Res. Microbiol.* 162 (5), 542-549.
41. Mitrano, D., Ranville, J., Bednar, A., Kazor, K., Hering, A., Higgins, C., 2014. Tracking dissolution of silver nanoparticles at environmentally relevant concentrations in laboratory, natural, and processed waters using single particle ICP-MS (spICP-MS). *Environ. Sci.: Nano* 1 (3), 248-259.
42. Mitrano, D M, Barber, A, Bednar, A, Westerhoff, P, Higgins, C P, Ranville, J F, 2012. Silver nanoparticle characterization using single particle ICP-MS (SP-ICP-MS) and asymmetrical flow field flow fractionation ICP-MS (AF4-ICP-MS). *J. Anal. Atom. Spectrom.* 27 (7), 1131-1142.
43. Mitzel, M.R., Tufenkji, N., 2014. Transport of industrial PVP-stabilized silver nanoparticles in saturated quartz sand coated with *Pseudomonas aeruginosa* PAO1 biofilm of variable age. *Environ. Sci. Technol.* 48 (5), 2715-2723.
44. Mohanta, Y.K., Panda, S.K., Bastia, A.K. and Mohanta, T.K., 2017. Biosynthesis of silver nanoparticles from *Protium serratum* and investigation of their potential impacts on food safety and control. *Front.Microbiol.* 8, 626.
45. Morones, J.R., Elechiguerra, J.L., Camacho, A., Holt, K., Kouri, J.B., Ramírez, J.T., Yacaman, M.J., 2005. The bactericidal effect of silver nanoparticles. *Nanotechnology* 16 (10), 2346.
46. Navarro, E., Piccapietra, F., Wagner, B., Marconi, F., Kaegi, R., Odzak, N., Sigg, L., Behra, R., 2008. Toxicity of silver nanoparticles to *Chlamydomonas reinhardtii*. *Environ. Sci. Technol. 42* (23), 8959-8964.
47. OECD, 1976. Proposed method for the determination of the biodegradability of surfactants used in synthetic detergents. Organisation for Economic Co-operation and Development, Paris, France.
48. Pace, H.E., Rogers, N.J., Jarolimek, C., Coleman, V.A., Gray, E.P., Higgins, C.P., Ranville, J.F., 2012. Single particle inductively coupled plasma-mass spectrometry: a performance evaluation and method comparison in the determination of nanoparticle size. *Environ. Sci. Technol.* 46(22), 12272-12280.

699 49. Park, E.J., Yi, J., Kim, Y., Choi, K., Park, K., 2010. Silver nanoparticles induce cytotoxicity
700 by a Trojan-horse type mechanism. *Toxicol. in vitro* 24(3), 872-878.
701 50. Park, H.-J., Park, S., Roh, J., Kim, S., Choi, K., Yi, J., Kim, Y., Yoon, J., 2013. Biofilm-
702 inactivating activity of silver nanoparticles: a comparison with silver ions. *J. Ind. Eng. Chem.*
703 19 (2), 614-619.
704 51. Patlolla, A.K., Berry, A., May, L., Tchounwo, P.B., 2012. Genotoxicity of silver
705 nanoparticles in *Vicia faba*: a pilot study on the environmental monitoring of nanoparticles.
706 *Int. J. Environ. Res. Public Health* 9(5), 1649-1662
707 52. Peulen, T.-O., Wilkinson, K.J., 2011. Diffusion of nanoparticles in a biofilm. *Environ. Sci.*
708 *Technol.* 45 (8), 3367-3373.
709 53. Song, J.E., Phenrat, T., Marinakos, S., Xiao, Y., Liu, J., Wiesner, M.R., Tilton, R.D., Lowry,
710 G.V., 2011. Hydrophobic interactions increase attachment of gum arabic-and PVP-coated Ag
711 nanoparticles to hydrophobic surfaces. *Environ. Sci. Technol.* 45 (14), 5988-5995.
712 54. Stewart, P S, Franklin, M J, 2008. Physiological heterogeneity in biofilms. *Nat. Rev.*
713 *Microbiol. 6*(3), 199-210.
714 55. Wirth, S.M., Lowry, G.V., Tilton, R.D., 2012. Natural organic matter alters biofilm tolerance
715 to silver nanoparticles and dissolved silver. *Environ. Sci. Technol.* 46 (22), 12687-12696.
716 56. Yang, Y., Quensen, J., Mathieu, J., Wang, Q., Wang, J., Li, M., Tiedje, J.M., Alvarez, P.J.,
717 2014. Pyrosequencing reveals higher impact of silver nanoparticles than Ag^+ on the
718 microbial community structure of activated sludge. *Water Res.* 48, 317-325
719 57. You, F., Tang, W., Yung, L.-Y.L., 2018. Real-time monitoring of the Trojan-horse effect of
720 silver nanoparticles by using a genetically encoded fluorescent cell sensor. Nanoscale 10(16),
721 7726-7735.
722 58. Young, B., Banihashemi, B., Forrest, D., Kennedy, K., Stintzi, A., Delatolla, R., 2016. Meso
723 and micro-scale response of post carbon removal nitrifying MBBR biofilm across carrier
724 type and loading. *Water Res.* 91, 235-243.
725 59. Yuan, Z.-H., Yang, X., Hu, A., Yu, C.-P., 2015. Long-term impacts of silver nanoparticles in
726 an anaerobic–anoxic–oxic membrane bioreactor system. *Chem. Eng. J.* 276, 83-90.
727 60. Zhang, C., Hu, Z., Li, P., Gajaraj, S., 2016a. Governing factors affecting the impacts of silver
728 nanoparticles on wastewater treatment. *Sci. Total Environ.* 572, 852-873.
729 61. Zhang, C., Liang, Z., Hu, Z., 2014. Bacterial response to a continuous long-term exposure of
730 silver nanoparticles at sub-ppm silver concentrations in a membrane bioreactor activated
731 sludge system. *Water Res.* 50, 350-358.
732 62. Zhang, W., Liu, X., Bao, S., Xiao, B., Fang, T., 2016b. Evaluation of nano-specific toxicity
733 of zinc oxide, copper oxide, and silver nanoparticles through toxic ratio. *J. Nanopart. Res.* 18
734 (12), 372.
735 63. Zhang, W., Xiao, B., Fang, T., 2018. Chemical transformation of silver nanoparticles in
736 aquatic environments: mechanism, morphology and toxicity. *Chemosphere* 191, 324-334.
737 64. Zhang, Z., Gao, P., Li, M., Cheng, J., Liu, W., Feng, Y., 2016c. Influence of Silver
738 nanoparticles on nutrient removal and microbial communities in SBR process after long-term
739 exposure. *Sci.Total Environ.* 569, 234-243.
740

List of Figures

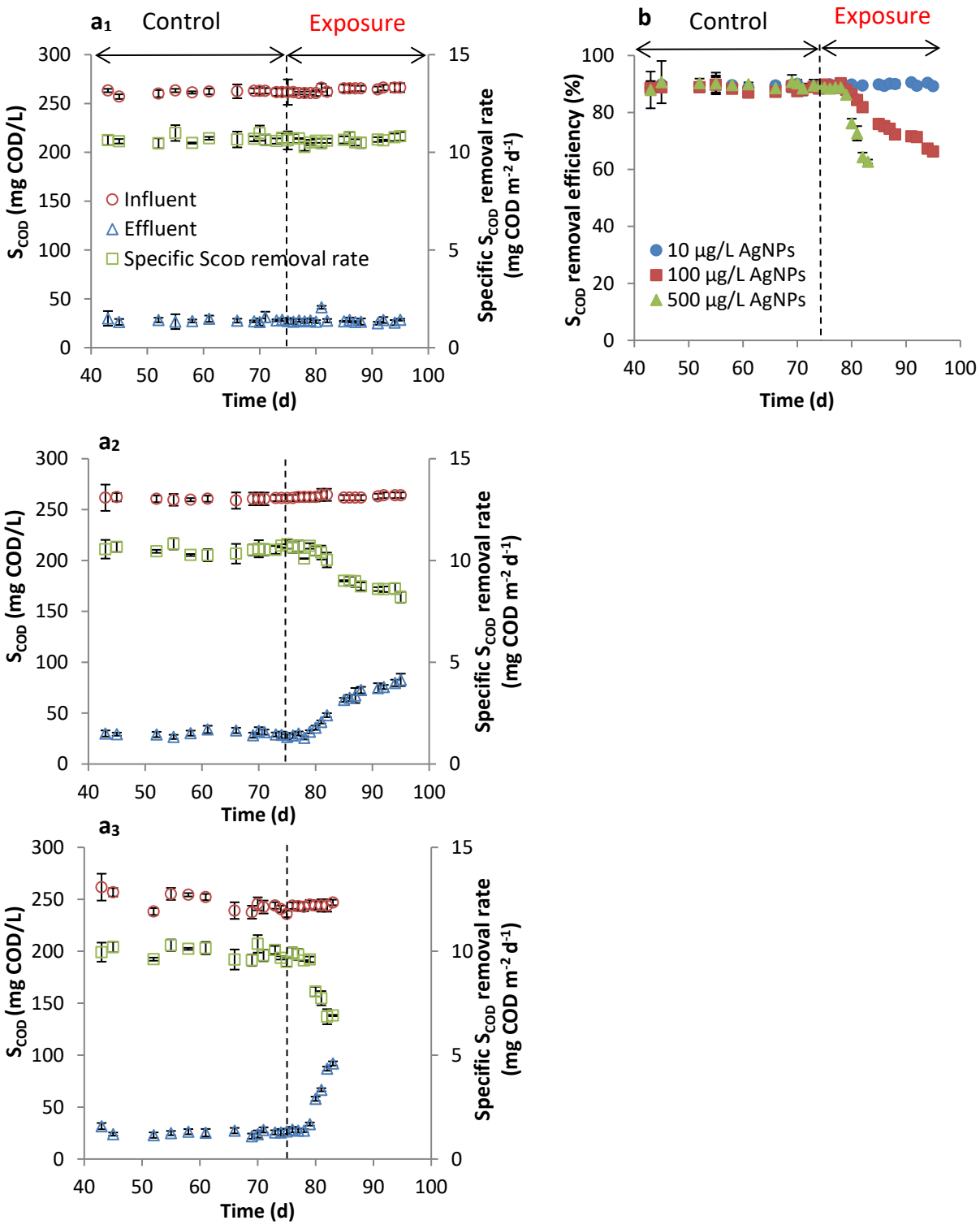

Fig 1. Effect of PVP-AgNPs on MBBR performance at (a_1) 10 µg/L AgNPs (a_2) 100 µg/L AgNPs, (a_3) 500 µg/L AgNPs and (b) S_{COD} removal efficiency

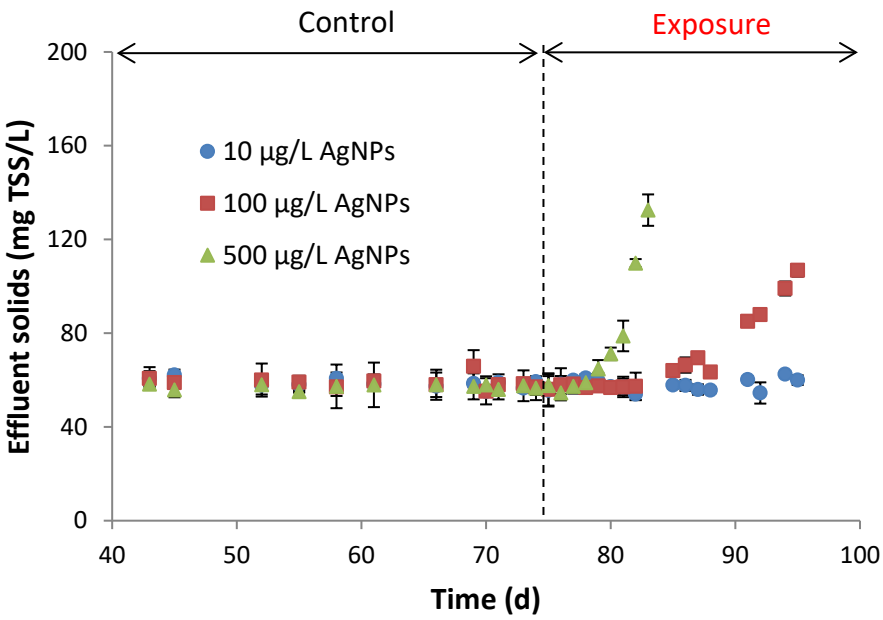

Fig 2. Effect of AgNPs on MBBR TSS_{eff}

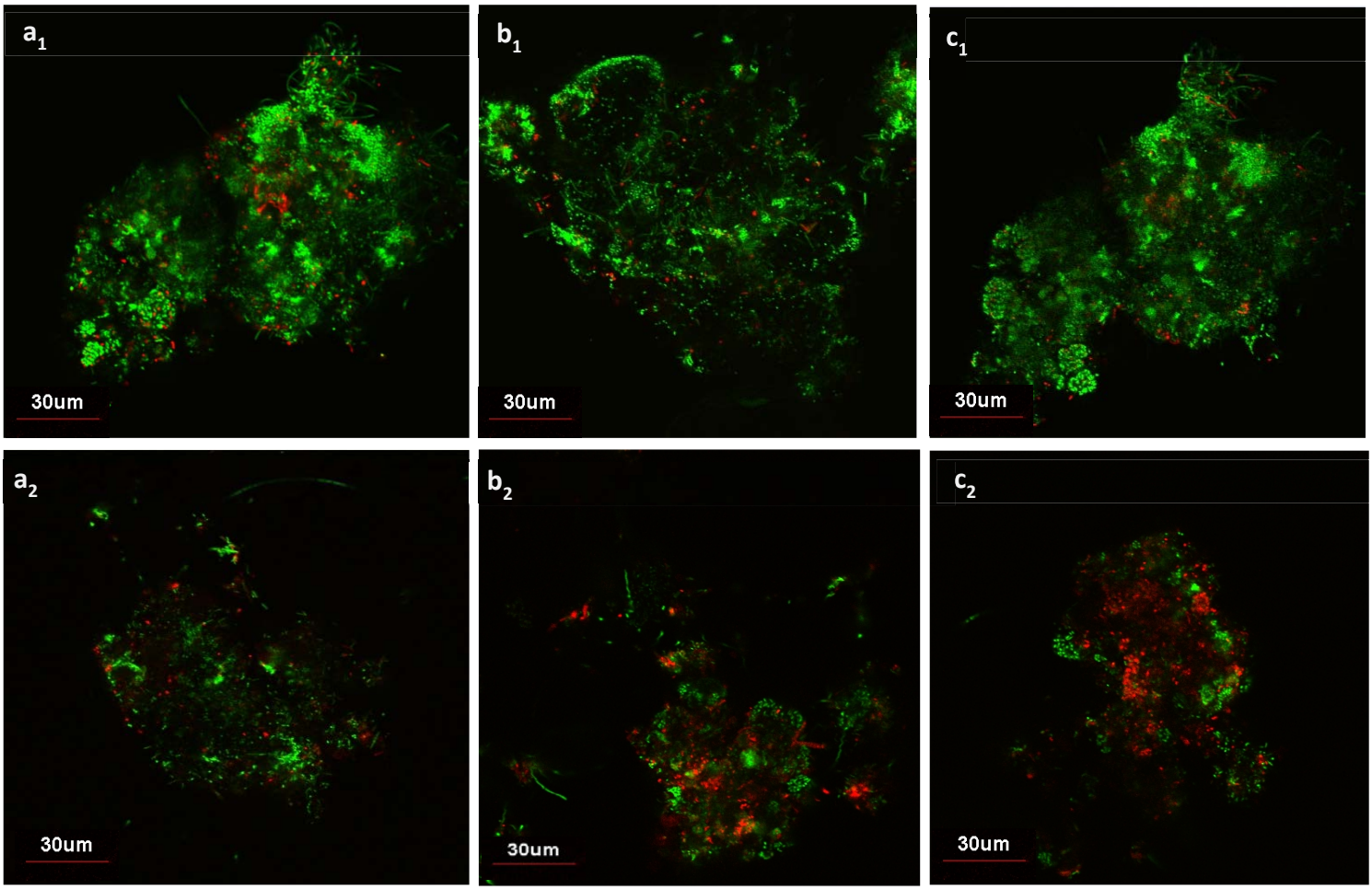

Fig 3.CLSM image of biofilm in the absence of AgNPs (a_1-c_1) and presence of 10 µg/L (a_2) and 100 µg/L of AgNPs (b_2) after 18 days exposure and 500 µg/L AgNPs (c_2) after 5 days exposure

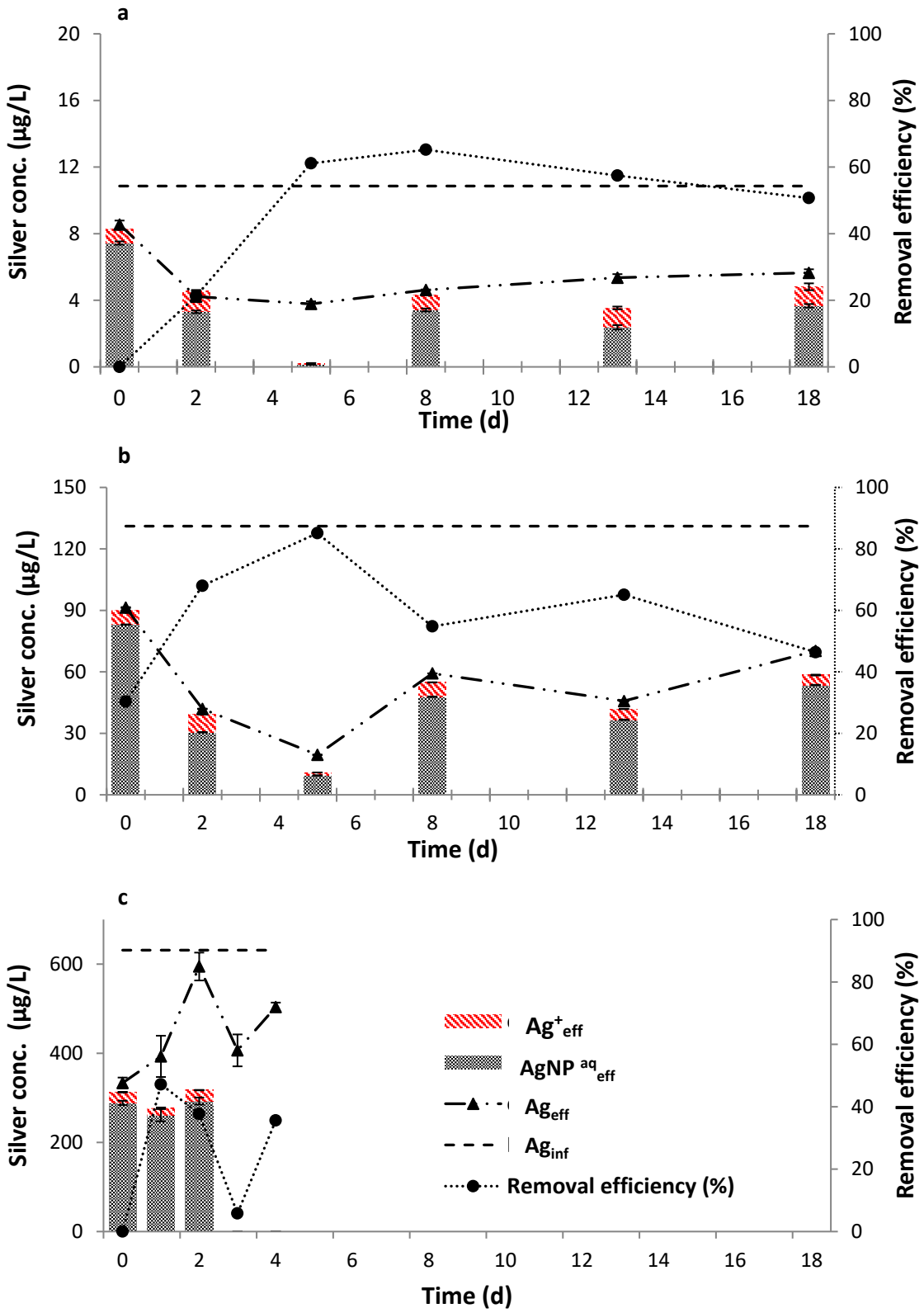

Fig 4. (a-c) Fate and removal of Ag in MBBRs

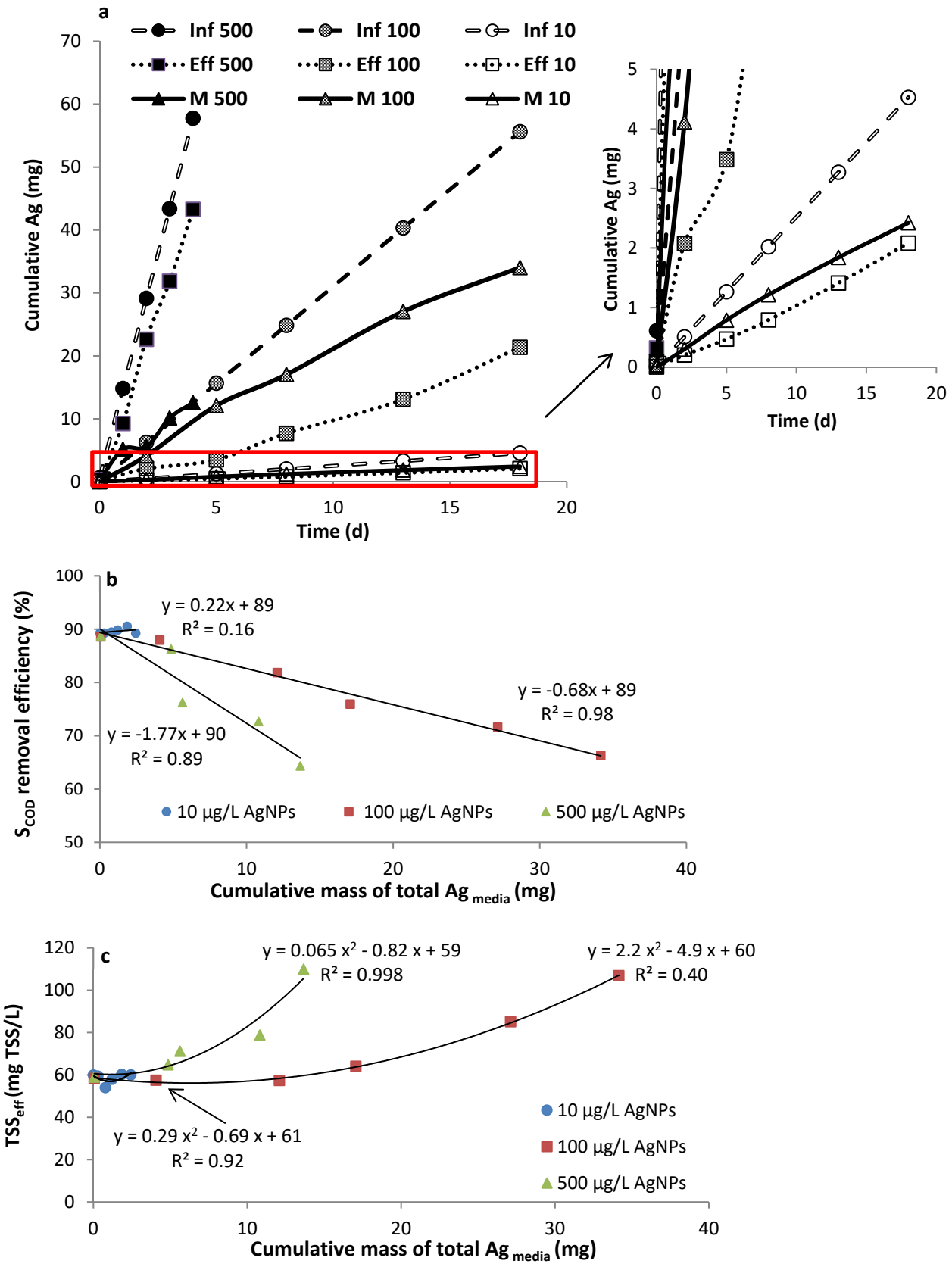

Fig 5. (a) Cumulative silver mass balance, (b) correlation between S_{COD} removal efficiency and mass of total Ag $_{media}$,(c) correlation between effluent solids and mass of total Ag $_{media}$

Note: negligible suspended Ag

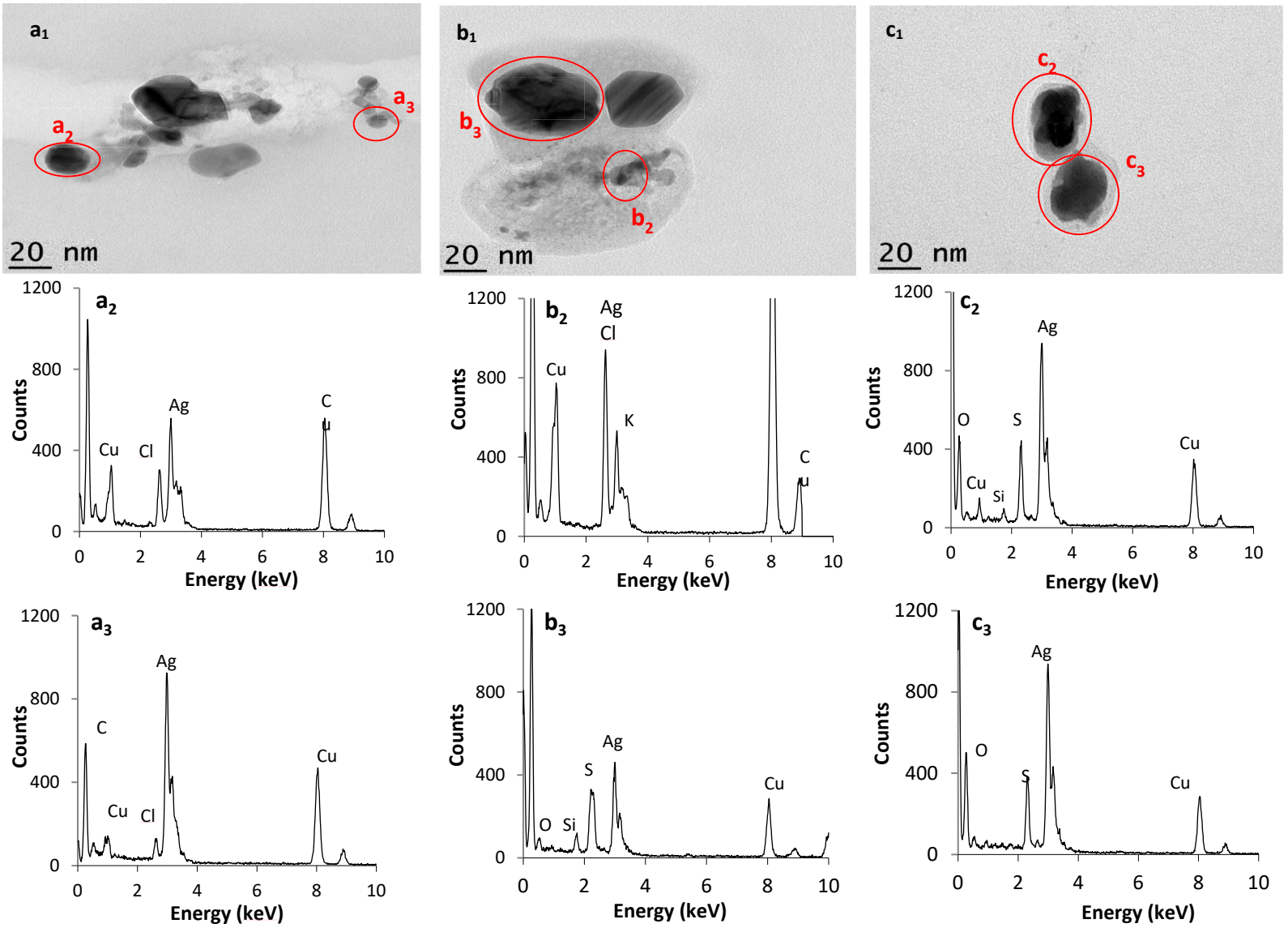

Fig 6.TEM images of the AgNPs in effluent of MBBR receiving (a_1) 10 µg/L (b_1) 100 µg/L and (c_1) 500 µg/L AgNPs and (a_2-c_3) the EDS analysis of the AgNPs

Analytical methodology

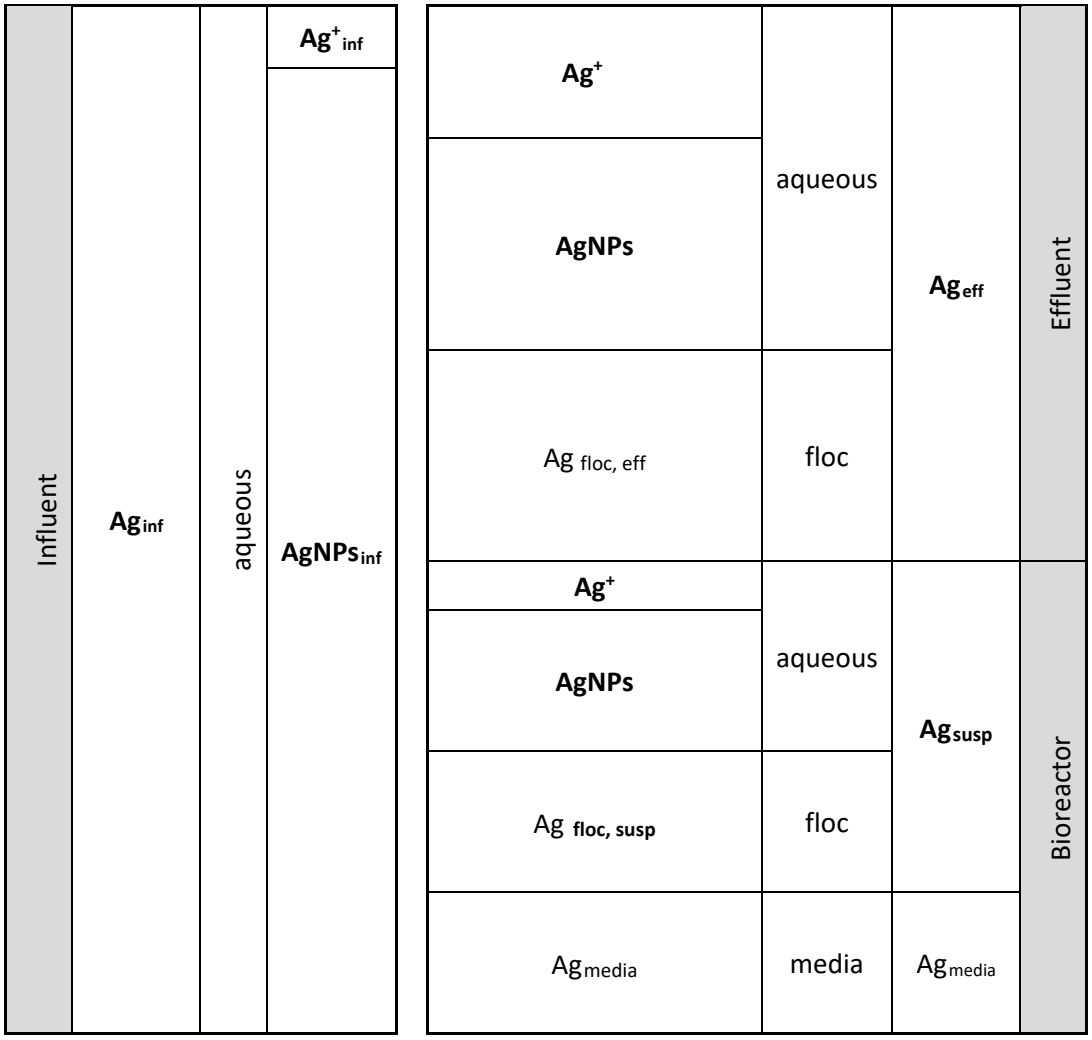

Note: susp: suspended biomass; bold characters for measured parameters

Fractionation of Ag in influent, effluent and bioreactor